SUPPLEMENTARY INFORMATION

Two-quartet kit* G-quadruplex is formed via double-stranded pre-folded structure

Anita Kotar[1], Riccardo Rigo[2], Claudia Sissi[2,*] and Janez Plavec[1,3,4,*]

[1] Slovenian NMR Center, National Institute of Chemistry, SI-1000, Ljubljana, Slovenia,
[2] Department of Pharmaceutical and Pharmacological Sciences, University of Padova, 35131 Padova, Italy
[3] Faculty of Chemistry and Chemical Technology, University of Ljubljana, Ljubljana, Slovenia and
[4] EN-FIST Center of Excellence, Ljubljana, Slovenia

* To whom correspondence should be addressed. Tel: +386 1 4760353; Fax: +386 1 4760300; Email: janez.plavec@ki.si. Correspondence may also be addressed to Claudia Sissi. Tel: +39 049 827 5711; Fax: +39 049 827 5366; Email: claudia.sissi@unipd.it.

MATERIALS AND METHODS

Circular dichroism (CD) spectroscopy

CD titrations were performed by increasing concentrations of KCl or LiCl in solution of oligonucleotide at 25 °C. After each titration step the system was left to equilibrate before spectra acquisition. CD signal variations at the maximum (for titration with K^+ ions monitored at 294 nm, while in Li^+ ions at 266 nm) were plotted as a function of the concentration of cations. Data points were fitted by applying one-site saturation model.

$$\theta_i = \frac{\theta_\infty \cdot [M^+]}{K_D + [M^+]} \qquad \text{Equation 1}$$

where $[M^+]$ is the cation concentration, θ_i is the signal at $[M^+]$, θ_∞ is the signal at the saturation and K_D is the dissociation constant.

For CD kinetic experiment, KCl was added manually to the cuvette from a stock solution and mixing was provided by an in-cuvette magnetic stirring bar. After a mixing time of 10 s, spectra acquisition was initiated using an interval scan of 30 min. The temperature was maintained at 37 °C. Data related to the folding process of kit*17 were analyzed by means of SVD analysis (1,2). The D matrix, defined by the optical signals in the whole wavelength range (rows) acquired at each single temperature (columns), was divided into three submatrices U, S, V, so that D = U x S x V. The singular values in S matrix and the autocorrelation coefficients of the U and V matrices give information about the number of species in solution that contribute to the signal variation. Significant U and V autocorrelation coefficients values above 0.75 were considered. Significant V eingenvectors in V matrix were globally fitted by applying different kinetic model and the best fitting was obtained by applying mono-exponential kinetic model,

$$\theta_t = a + b \cdot e^{(t/\tau)} \qquad \text{Equation 2}$$

where θ_t is CD signal at time t, a and b are fitting parameters and τ is the relaxation time of the process.

The fitting parameters formed the H matrix. By multiplying the H matrix for the U x S matrix, the actual shapes of the dichroic signals of species in solution were obtained.

CD melting studies were performed on kit* and kit*17. The experiments were carried out between 25 and 95°C in 150 mM KCl. The heating rate was 50°C/hour where at each 2°C the temperature was held for 5 minutes and the corresponding CD signal was recorded at 294 and 264 nm for kit* and kit*17, respectively. The melting profile of kit* that shows only one fully reversible melting transition was analyzed by fitting the signal variation according to a single-transition model based on van't Hoff formalism (3,4),

$$\theta_T = \frac{u * e^{-\left(\frac{\Delta H}{RT} * \left(\left(\frac{T}{Tm}\right) - 1\right)\right)} + l}{e^{-\left(\frac{\Delta H}{RT} * \left(\left(\frac{T}{Tm}\right) - 1\right)\right)} + 1} \qquad \text{Equation 3}$$

where T is temperature, θ_T is the CD signal at temperature T, u and l are fitting parameters, ΔH is the enthalpy of the unfolding process, R is the ideal gas constant and Tm is the melting temperature of the folded oligonucleotide.

The melting profile of kit*17, presenting two distinct melting transitions, was analyzed by using a two-transitions model based on van't Hoff formalism (3,4),

$$\theta_T = \frac{u * e^{-\left(\frac{\Delta H1}{RT} * \left(\left(\frac{T}{Tm1}\right) - 1\right) + \frac{\Delta H2}{RT} * \left(\left(\frac{T}{Tm2}\right) - 1\right)\right)} + a * e^{-\left(\frac{\Delta H1}{RT} * \left(\left(\frac{T}{Tm1}\right) - 1\right)\right)} + l}{e^{-\left(\frac{\Delta H1}{RT} * \left(\left(\frac{T}{Tm1}\right) - 1\right) + \frac{\Delta H2}{RT} * \left(\left(\frac{T}{Tm2}\right) - 1\right)\right)} + e^{-\left(\frac{\Delta H1}{RT} * \left(\left(\frac{T}{Tm1}\right) - 1\right)\right)} + 1} \qquad \text{Equation 4}$$

where T is temperature, θ_T is the CD signal at temperature T, u, a and l are fitting parameters, $\Delta H1$ and $\Delta H2$ are the enthalpies associated to each melting step, R is the ideal gas constant, T_{m1} and T_{m2} are the melting temperatures.

UV spectroscopy

UV melting experiments were recorded on a Varian CARY-100 BIO UV-VIS spectrophotometer (Varian Inc.) equipped with a thermoelectric temperature controller at 20 μM concentration of oligonucleotides per strand in 20 mM potassium phosphate buffer (pH 7.4) and 100 mM KCl. Folding/unfolding processes were followed between 10 and 95 °C by measuring absorbance at 260 and 295 nm using scanning rate of 0.5 °C min^{-1}. Data points were fitted by applying Equations 3 and 4.

Fluorescence spectroscopy

Acrylamide quenching experiments were performed on previously folded oligonucleotides in 150 mM KCl. The quenching efficiency was monitored at 370 nm at 25°C and plotted as a function of the acrylamide concentration. Data points were fitted according to Stern-Volmer formalism to obtain quenching parameters. Linear quenching correlation was analyzed using a one-component system model (5),

$$\frac{F_0}{F_Q} = 1 + K_{sv} \cdot [Q] \qquad \text{Equation 5}$$

where [Q] is the acrylamide concentration, F_0 is the initial value of fluorescence, F_Q is the fluorescence signal at [Q] and K_{sv} is the Stern-Volmer constant.

Non-linear quenching correlation was analyzed according to a two-component system model (5),

$$\frac{F_Q}{F_0} = \frac{f}{1 + K_{sv,1} \cdot [Q]} + \frac{1 - f}{1 + K_{sv,2} \cdot [Q]} \qquad \text{Equation 6}$$

where [Q] is the acrylamide concentration, F_0 is the initial value of fluorescence, F_Q is the fluorescence signal at [Q], f is the accessible fluorophore fraction, $K_{sv,1}$ and $K_{sv,2}$ are the Stern-Volmer constants.

Polyacrylamide gel electrophoresis (PAGE)

A solution containing 3 μM kit* labelled with 6-FAM at 3'-end and 500 μM kit* (not labelled) in 10 mM TRIS, 100 mM KCl, pH 7.5 was incubated at room temperature for 1 h. Then the sample was loaded on a native 15% polyacrylamide gel (19:1 acrylamide: bisacrylamide) in 1× TBE and the gel was run at 10 °C for 3 h at 150 V. 22 and 44 bases long Scrambled oligonucleotides (22b, 5′-GGATGTGAGTGTGAGTGTGAGG-6-FAM-3′; 44b 5′-GGATGTGAGTGTGAGTGTGAGG GGATGTGAGTGTGAGTGTGAGG-6-FAM-3) were used as electrophoretic mobility markers. The resolved bands were visualized on an image acquisition system (Geliance 600 Imaging system, Perkin-Elmer).

Structure calculations and molecular dynamics simulations

The structures of kit* G-quadruplex were calculated by the simulated annealing (SA) simulations. The force field parameters were adopted from the Generalized Amber force field (6). SA simulations were performed using the CUDA version of pmemd module of AMBER 14 program suites (7,8) and Cornell et al. force field basic version parm99 (9) with the bsc0 (10), χOL4 (11), ε/ζOL1 (12) and βOL1 (13) refinements. The initial extended single-stranded DNA structure was obtained using the leap module of AMBER 14. A total of 100 structures were calculated in 80 ps of NMR restrained SA simulations using the generalized Born implicit model (14,15). The cut-off for non-bonded interactions was 999 Å and the SHAKE algorithm (16) for hydrogen atoms was used with the 0.4 fs time steps. For each SA simulation, a random velocity was used. The SA simulation was performed as described (17): in 0-2 ps, the temperature was raised from 300 K to 1000 K and held constant at 1000 K for 38 ps. Temperature was scaled down to 500 K in the next 24 ps and reduced to 100 K in the next 8 ps and was further reduced to 0 K in the last 8 ps. A family of 10 structures was selected based on the smallest restraints violations and lowest energy. Figures were visualized and prepared with UCSF Chimera (18).

Molecular dynamics simulations

For molecular dynamics simulations the kit* G-quadruplex was placed in a truncated octahedral box of TIP3P water molecules with the box border at least 10 Å away from any atoms of the G-quadruplex. Extra K^+ ions were added to neutralize the negative charges of the G-quadruplex. The force field for MD simulation was the same as for the SA simulation. The simulations were performed with the CUDA version of pmemd module of AMBER 14 (7,19-22). Prior to MD simulation, the system were subjected to a series of minimizations and equilibrations. The equilibration protocol started with 1000 steps of steepest descent minimization followed by 4000 steps of conjugate gradient minimization with 10 kcal mol^{-1} $Å^{-2}$ position restraints on DNA atoms. Then the whole system was minimized by 1000 steps of steepest descent minimization and 4000 steps of conjugate gradient minimization without restraint. The system was heated from 0 to 300 K during 100 ps with position restraints of 10 kcal mol^{-1} $Å^{-2}$ on

G-quadruplex. Afterwards, the system was equilibrated during 50 ps at constant temperature of 300 K and pressure of 1 atm with 2 kcal mol^{-1} $Å^{-2}$ restraints on DNA atoms. Finally, the system was equilibrated using starting velocities from the previous equilibration without position restraints. Pressure coupling used during equilibration was set to 0.2, coupling during the last molecular dynamics phase was set to 5. The production simulation were carried out at constant pressure of 1 atm and constant temperature of 300 K maintained using Langevin dynamics with a collision frequency of 2.0. Periodic boundary conditions were used, and electrostatic interactions were calculated by the particle mesh Ewald method (23,24) with the non-bonded cutoff set to 8 Å. The SHAKE algorithm (16) was applied to bonds involving hydrogens, and a 2 fs integration step was used. The production run was carried out for continuous 200 ns and the snapshots were written at every 1 ps. Three MD simulations were performed with different initial velocity distributions. Trajectories were analyzed using the CPPTRAJ module of AMBER.

RESULTS

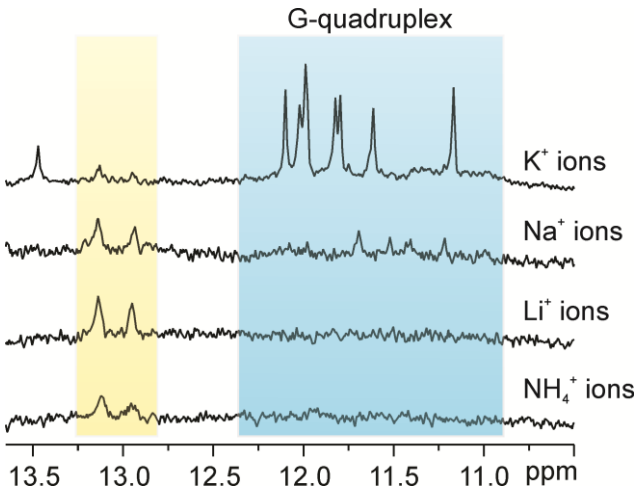

Figure S1. Imino region of ^{1}H NMR spectra of kit* in the presence of 100 mM concentration of K^{+}, Na^{+}, Li^{+} and NH_4^{+} ions as indicated on the right. ^{1}H NMR spectra were recorded in lithium cacodylate buffer (pH 7.2) at 0.3 - 0.5 mM kit* concentration per strand, 37°C on a 600 MHz NMR spectrometer. The region characteristic for imino signals of guanine residues involved in G-quartets is marked with blue. Signals of pre-folded state(s) of kit* are marked with yellow.

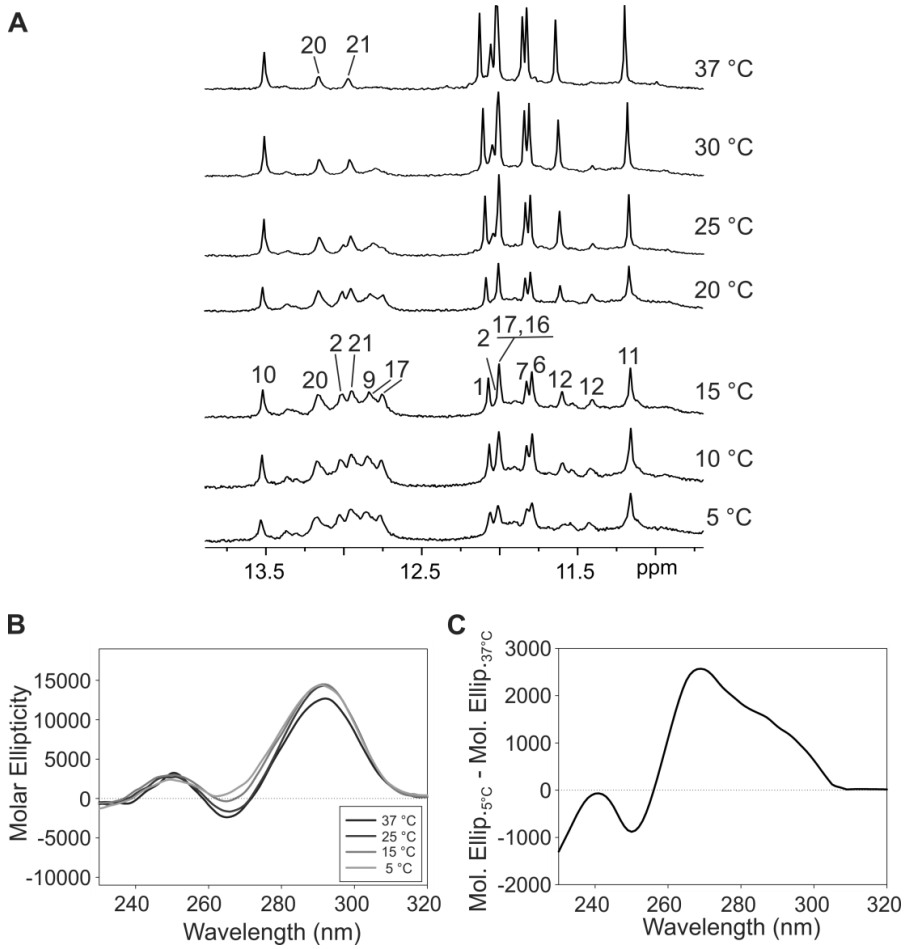

Figure S2. A) Imino region of ^{1}H NMR spectra of kit* between 5 and 37°C. Assignments are shown above individual signals. The NMR spectra were recorded at 0.5 mM kit* concentration per strand, 100 mM KCl, pH 7.4 on an 800 MHz NMR spectrometer. **B**) CD spectra of kit* in 100 mM KCl at different temperatures. **C**) CD signal of kit* at 5°C subtracted of the CD contribution at 37°C.

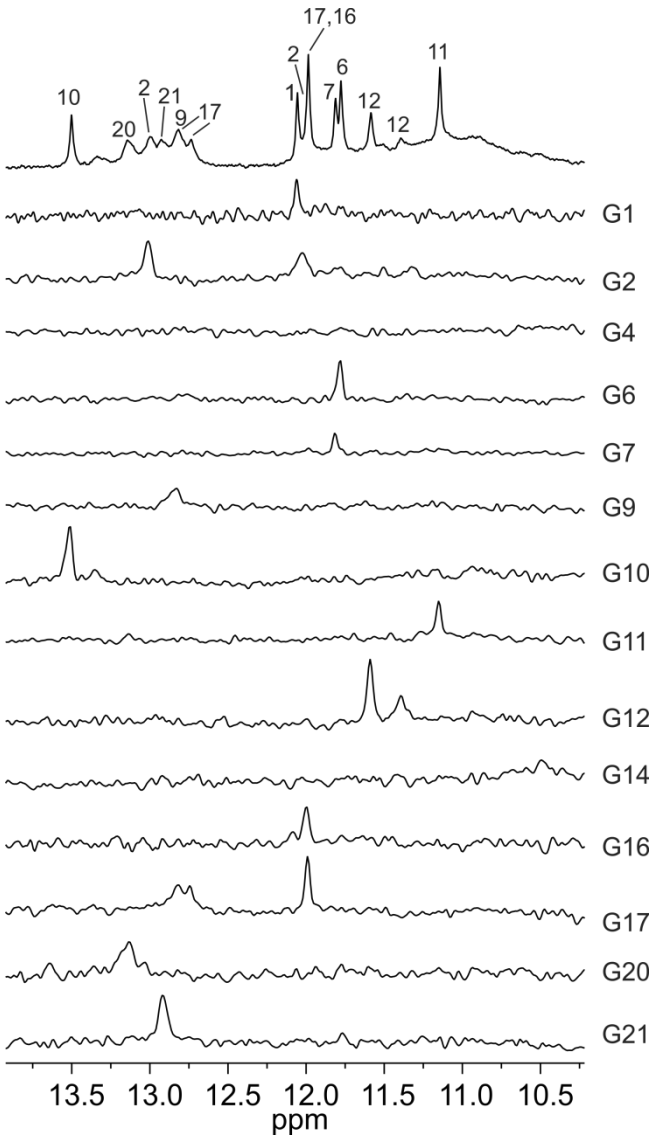

Figure S3. ^{1}H and 1D ^{15}N-edited HSQC NMR spectra of kit* at 15°C. The HSQC spectra were acquired on partially (10%) residue-specifically ^{15}N- and ^{13}C-labeled oligonucleotides. Assignment of H1 proton resonances is indicated on the right side of each 1D HSQC spectrum. NMR spectra were recorded at 0.5 mM kit* concentration per strand, 100 mM KCl, pH 7.4 on a 600 MHz NMR spectrometer.

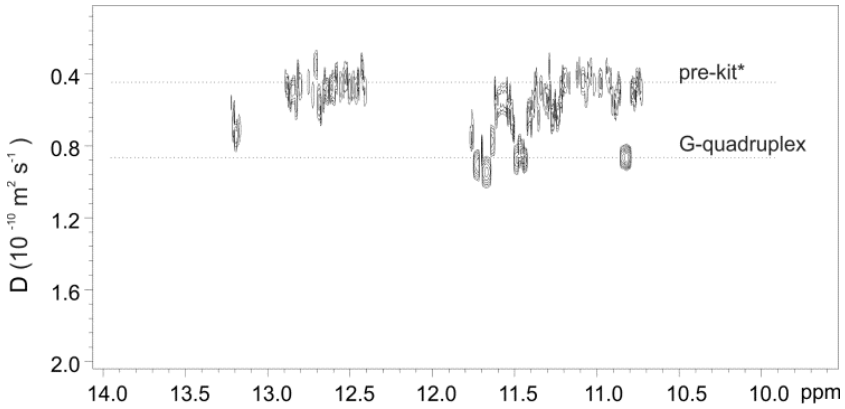

Figure S4. DOSY NMR spectrum of kit*. The determined translational diffusion coefficients were 0.87 x 10^{-10} for kit* G-quadruplex and 0.45 x 10^{-10} m^2 s^{-1} for pre-kit*. The NMR spectrum was recorded at 0.5 mM kit* concentration per strand, 100 mM KCl, pH 7.4, 5°C on a 600 MHz NMR spectrometer.

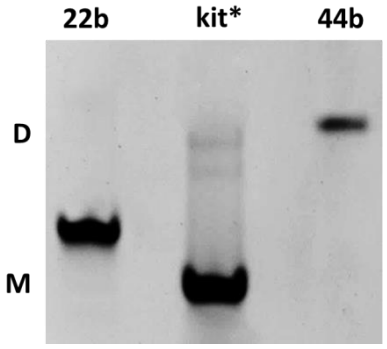

Figure S5. Distribution of kit* between monomeric and dimeric (pre-kit*) species. PAGE resolution of 500 µM kit* in 100 mM KCl, 10 mM TRIS, pH 7.5 performed on a 15% polyacrylamide gel in TBE 1x. 22b and 44b were electrophoretic mobility markers of 22 and 44 bases, respectively.

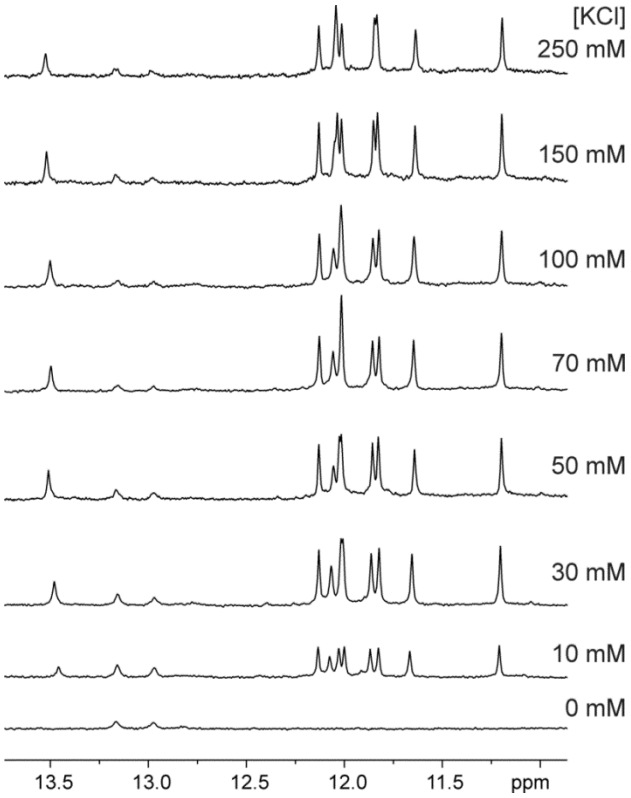

Figure S6. Imino region of ^{1}H NMR spectra of kit* at different concentrations of KCl indicated on the right. ^{1}H NMR spectra were recorded in potassium phosphate buffer (pH 7.4), at 0.4 mM kit* concentration per strand, 37°C on a 600 MHz NMR spectrometer.

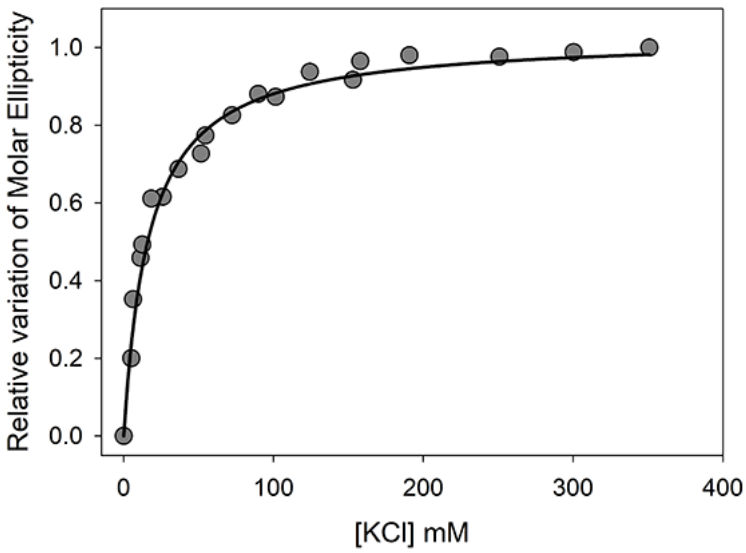

Figure S7. Relative variation of molar ellipticity obtained by monitoring the spectral changes induced by the addition of KCl at 294 nm. Data were fitted according to one-site saturation model (Equation 1).

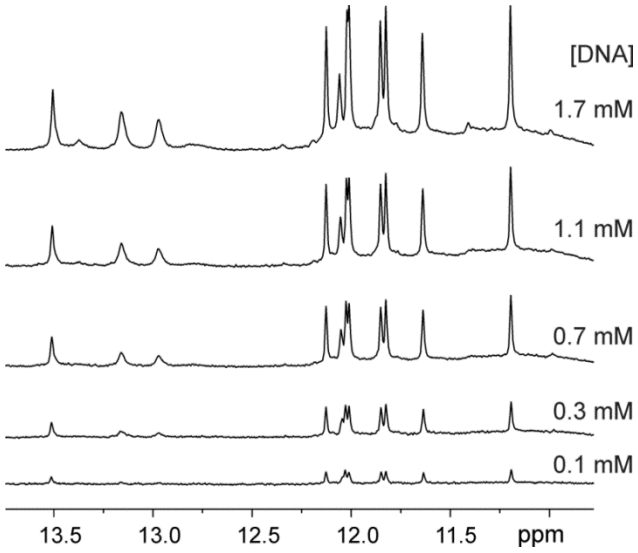

Figure S8. Imino region of ^{1}H NMR spectra of kit* in the presence of different concentrations per strand of kit* (DNA) as indicated on the right. ^{1}H NMR spectra were recorded in potassium phosphate buffer (pH 7.4), at 100 mM KCl, 37°C on a 600 MHz NMR spectrometer.

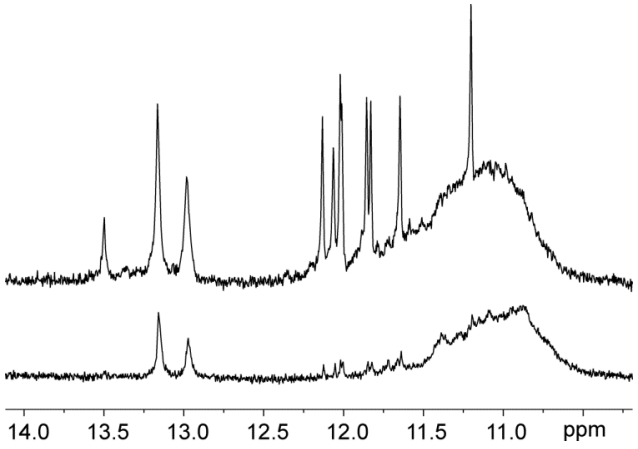

Figure S9. Imino region of ^{1}H NMR spectra of kit* before (top) and after (bottom) overnight annealing. ^{1}H NMR spectra were recorded at 2 mM kit* concentration per strand in potassium phosphate buffer (pH 7.4), at 100 mM KCl, 37°C on a 600 MHz spectrometer.

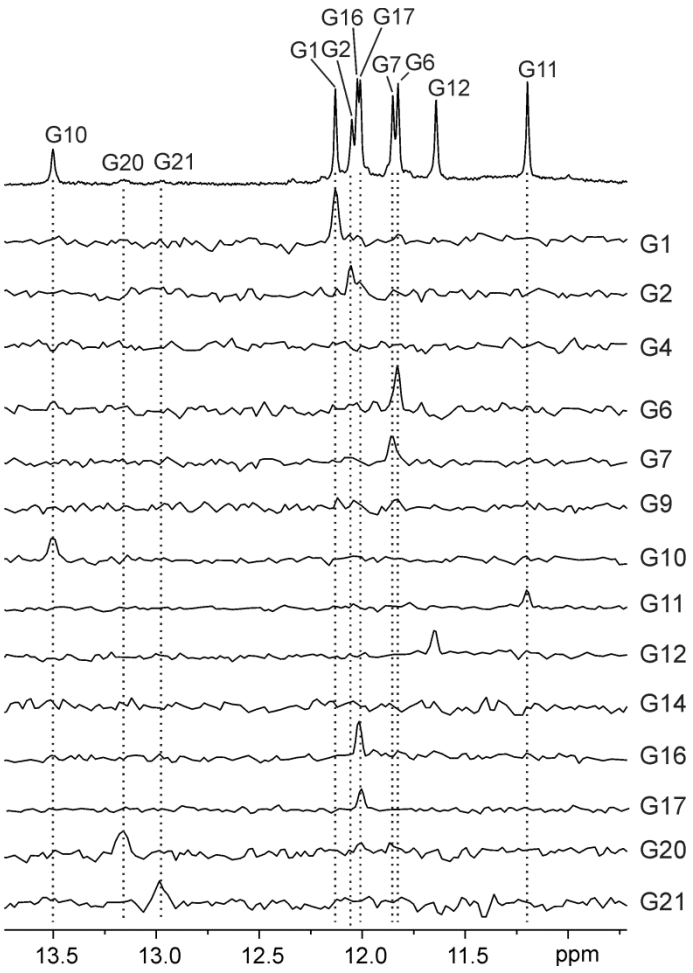

Figure S10. Imino region of ^{1}H and 1D ^{15}N-edited HSQC NMR spectra of kit* at 37°C. The HSQC spectra were acquired on partially (10%) residue-specifically ^{15}N- and ^{13}C-labelled oligonucleotides. Assignment of H1 proton resonances is indicated on the right of each 1D HSQC spectrum. NMR spectra were recorded at 0.5 mM kit* concentration per strand, 100 mM KCl, pH 7.4 on a 600 MHz spectrometer.

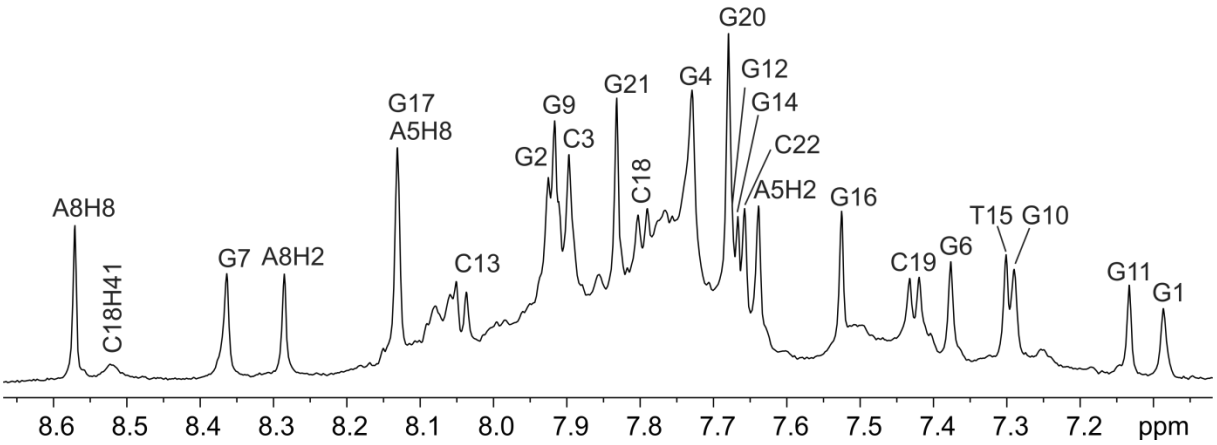

Figure S11. Aromatic region of ^{1}H NMR spectra of kit*. Assignments are shown above individual signals. NMR spectrum was recorded at 0.5 mM kit* concentration per strand, 100 mM KCl, pH 7.4, 37°C on a 600 MHz spectrometer.

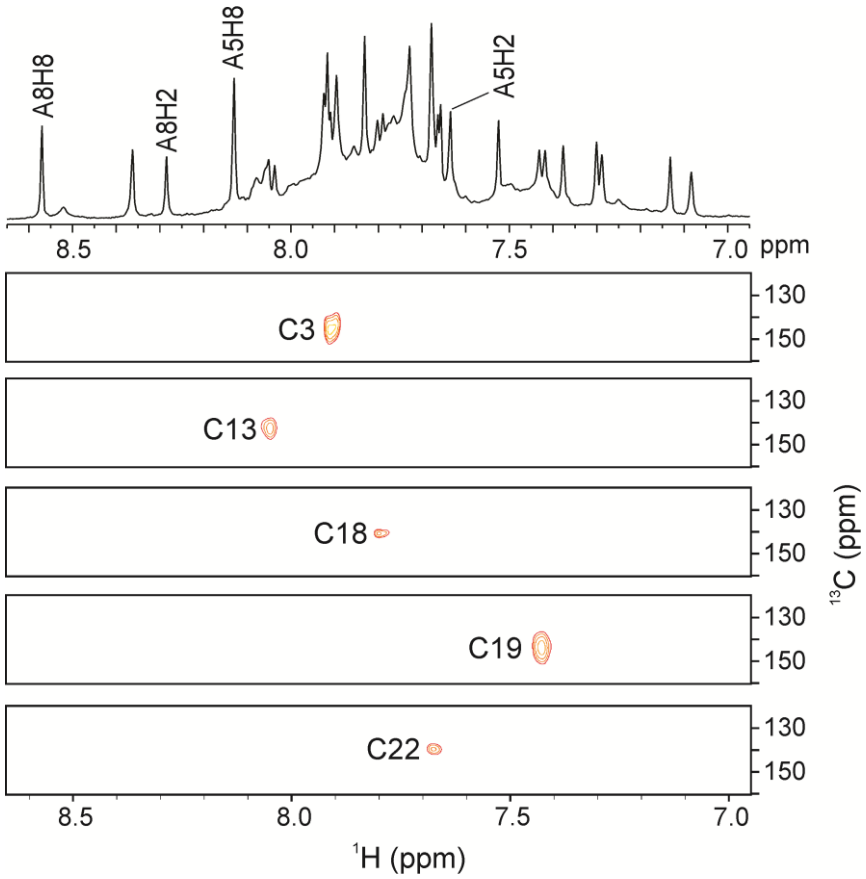

Figure S12. Aromatic region of 1D ^{1}H and 2D ^{13}C-edited HSQC NMR spectra of kit*. The HSQC spectra were acquired on partially (4%) residue-specifically ^{15}N- and ^{13}C-labeled oligonucleotides. Assignment of H6 proton resonances is indicated next to the 2D cross-peaks. The NMR spectra were recorded at 0.5 mM kit* concentration per strand, 100 mM KCl, pH 7.4, 37°C on a 600 MHz spectrometer.

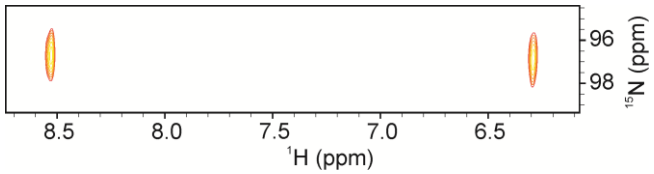

Figure S13. 2D ^{15}N-edited HSQC NMR spectrum of amino group of C18 residue of kit*. The HSQC spectrum was acquired on partially (4%) residue-specifically ^{15}N- and ^{13}C-labeled oligonucleotide. NMR spectrum was recorded at 0.5 mM kit* concentration per strand, 100 mM KCl, pH 7.4, 37°C on a 600 MHz spectrometer.

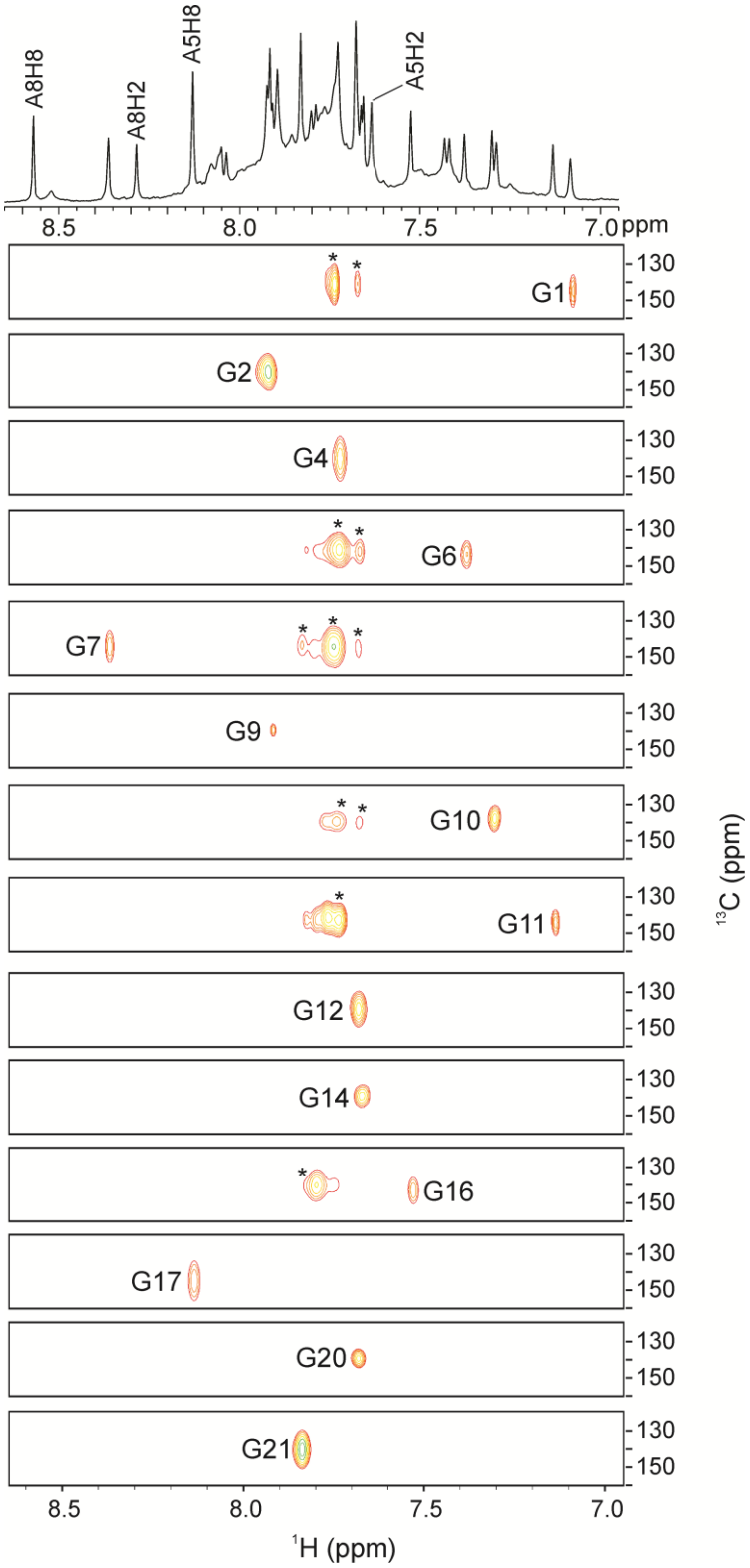

Figure S14. Aromatic region of 1D ^{1}H and 2D ^{13}C-edited HSQC NMR spectra of kit*. The HSQC spectra were acquired on partially (10%) residue-specifically ^{15}N- and ^{13}C-labeled oligonucleotides. Assignment of H8 proton resonances is indicated next to the 2D cross-peaks. With asterisks are marked signals that arise from unfolded or pre-folded oligonucleotide. NMR spectra were recorded at 0.5 mM kit* concentration per strand, 100 mM KCl, pH 7.4, 37°C on a 600 MHz spectrometer.

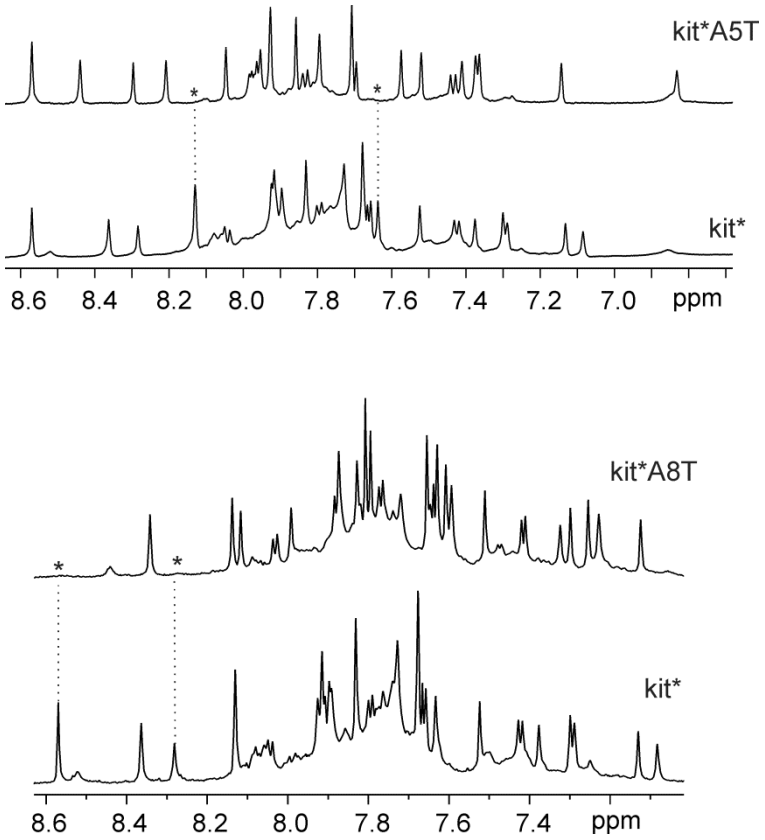

Figure S15. Aromatic region of ^{1}H NMR spectra of kit*A5T, kit*A8T and kit*. The missing aromatic signals of A5 in kit*A5T and A8 in kit*A8T are marked with asterisks. NMR spectra were recorded at 0.4 mM oligonucleotide concentration per strand, 100 mM KCl, pH 7.4, 37°C on 800 and 600 MHz spectrometers.

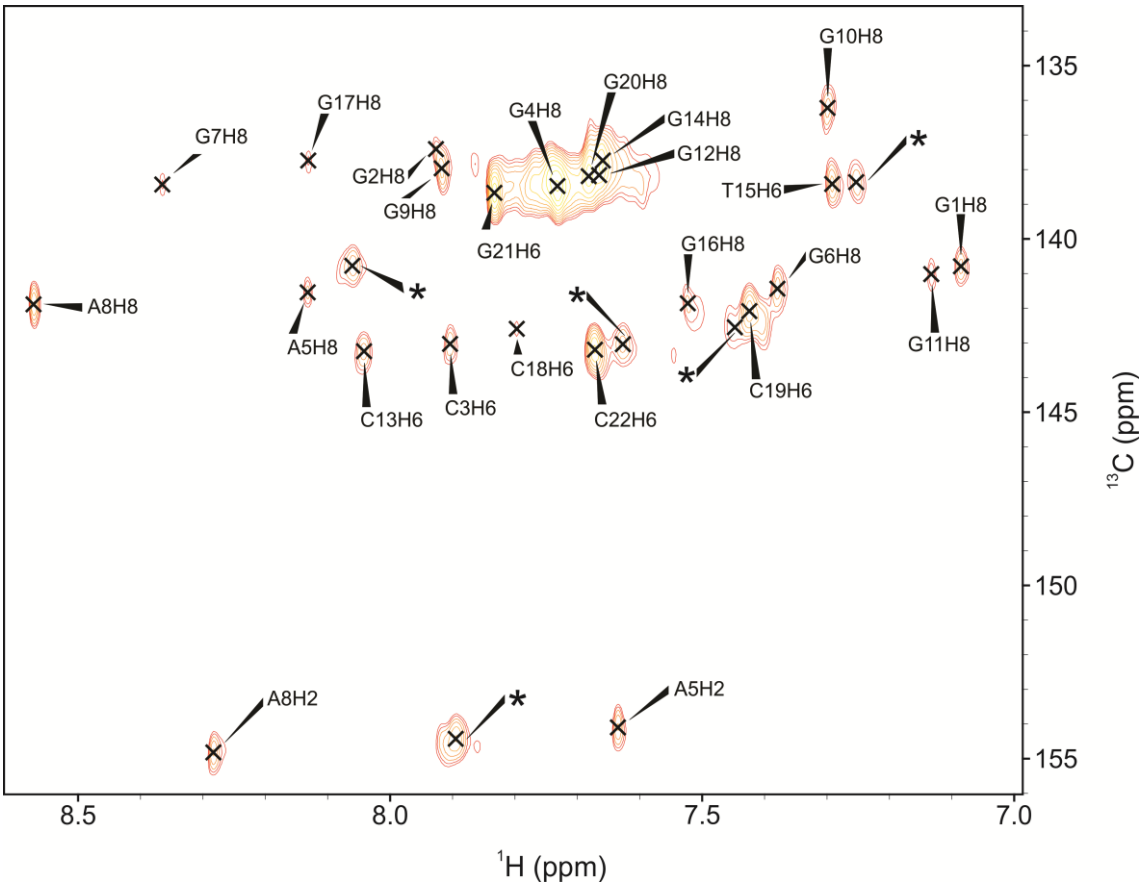

Figure S16. Aromatic region of 2D ^{1}H-^{13}C HSQC NMR spectrum of kit*. Assignment of individual cross-peaks is indicated. NMR spectrum was recorded at 0.4 mM kit* concentration per strand, 100 mM KCl, pH 7.4, 37°C on an 800 MHz spectrometer. The signals marked with asterisks arise from the pre-folded structure.

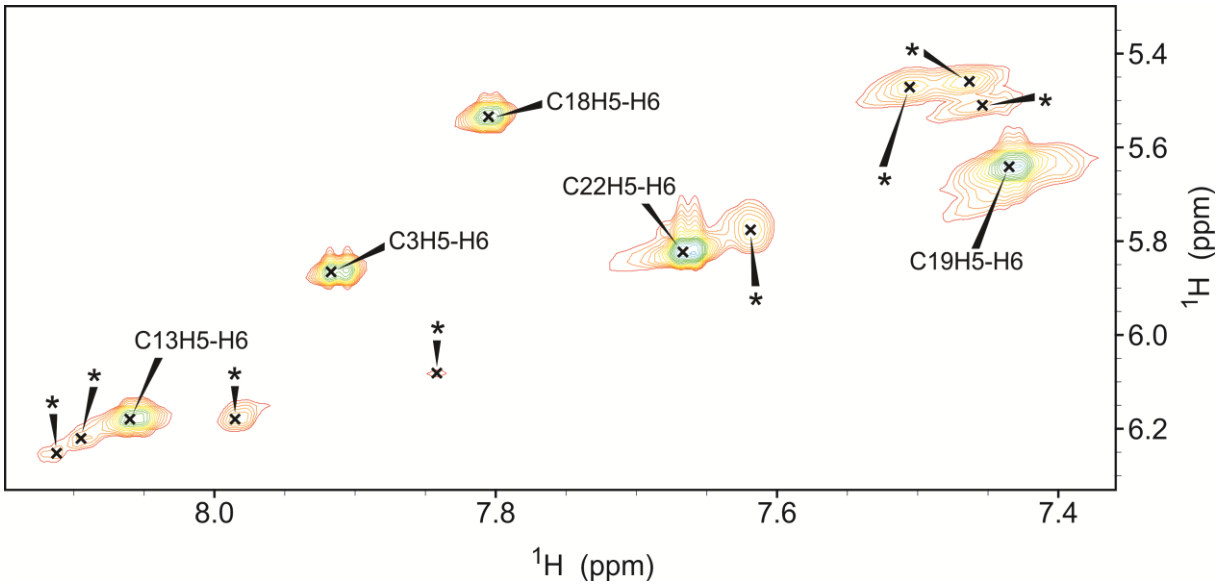

Figure S17. H6-H5 cross-peaks of cytosine residues in TOCSY spectrum (τ_m 80 ms) of kit*. Assignment of individual cross-peaks of kit* G-quadruplex is indicated. The cross-peaks belonging to pre-kit* are marked with asterisks. NMR spectrum was recorded at 0.4 mM kit* concentration per strand, 100 mM KCl, 100% ^2H_2O, 37°C on an 800 MHz spectrometer.

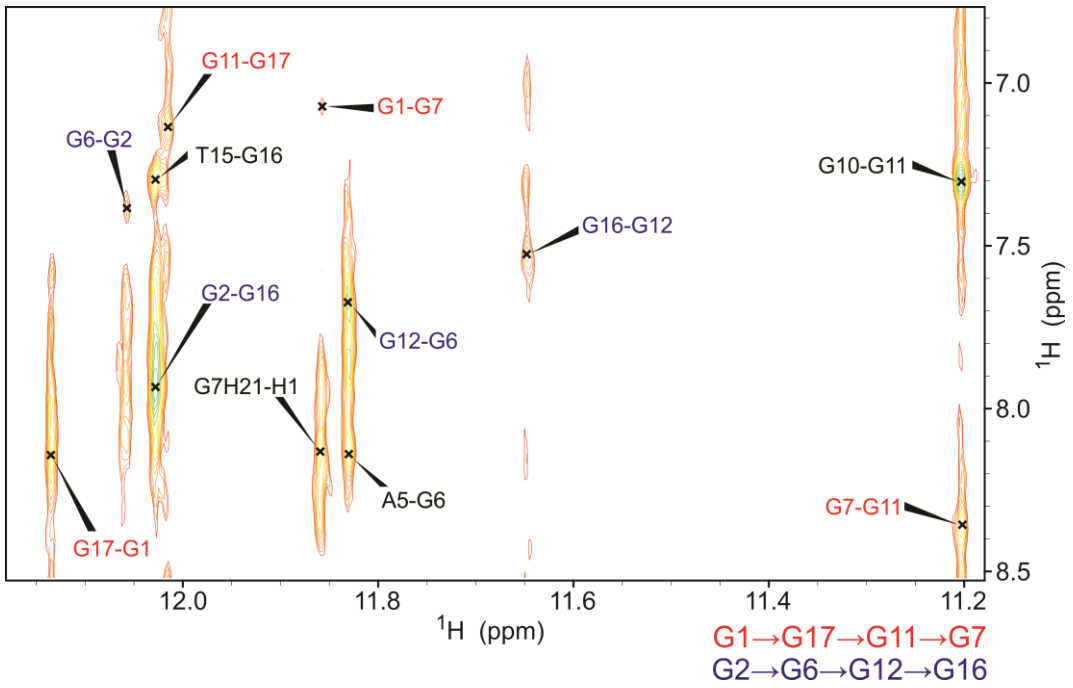

Figure S18. Imino-aromatic region of NOESY spectrum (τ_m 450 ms) of kit*. Cross-peaks identifying connectivities within G1-G17-G11-G7 and G2-G6-G12-G16 quartets are colored red and blue, respectively. With arrows are marked H1-H8 and G7H1-H21 connectivities. NMR spectrum was recorded at 0.5 mM kit* concentration per strand, 100 mM KCl, pH 7.4, 37°C on an 800 MHz spectrometer.

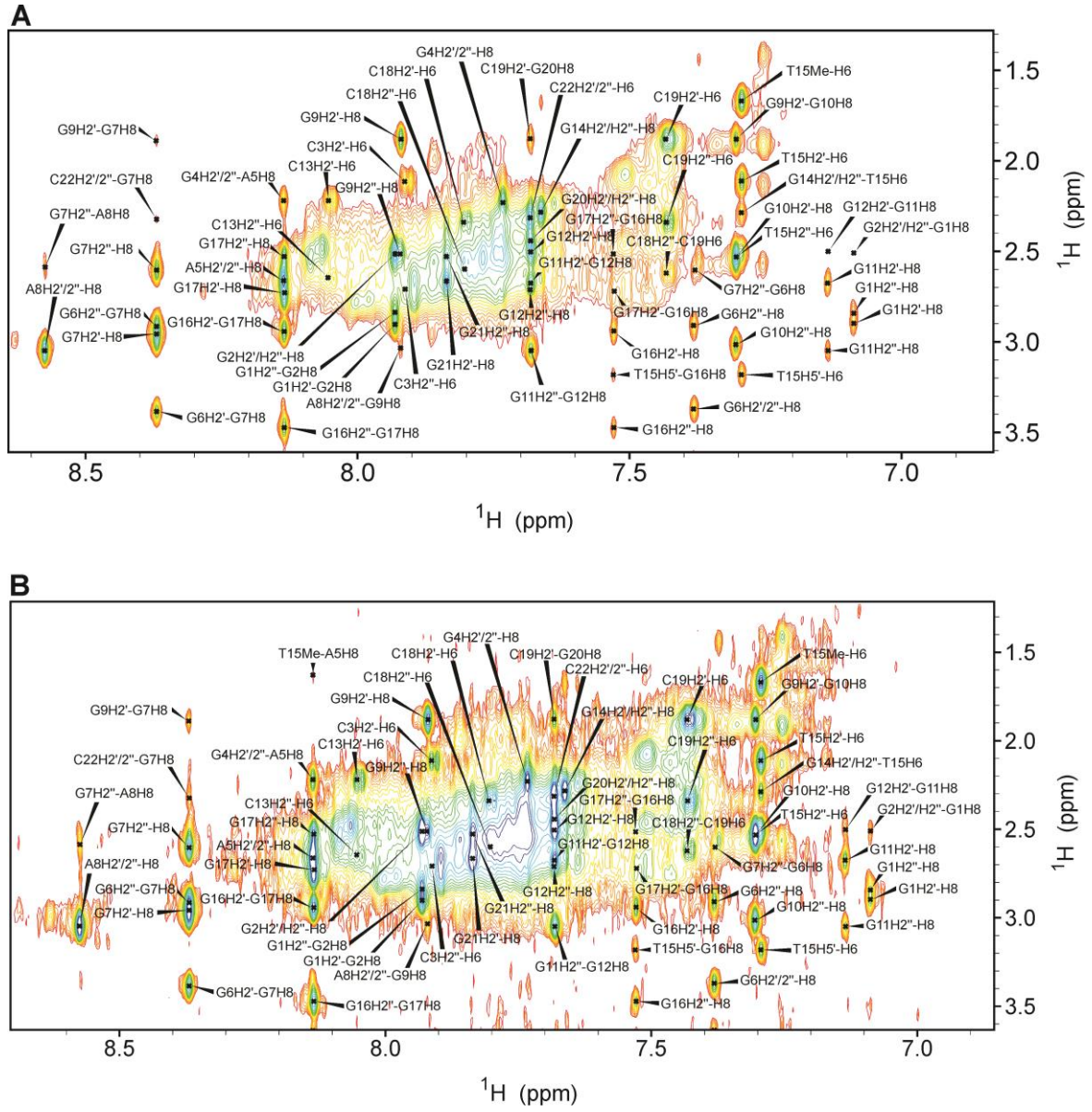

Figure S19. A) Aromatic-H2'/H2" region of NOESY spectrum (τ_m 450 ms) of kit*. **B**) Aromatic-H2'/H2" region of NOESY spectrum with 2..5 lover level of contours compared to **A**) to present cross-peak between A8 H8 and T15 Me. NMR spectrum was recorded at 0.5 mM kit* concentration per strand, 100 mM KCl, pH 7.4, 37°C on an 800 MHz spectrometer.

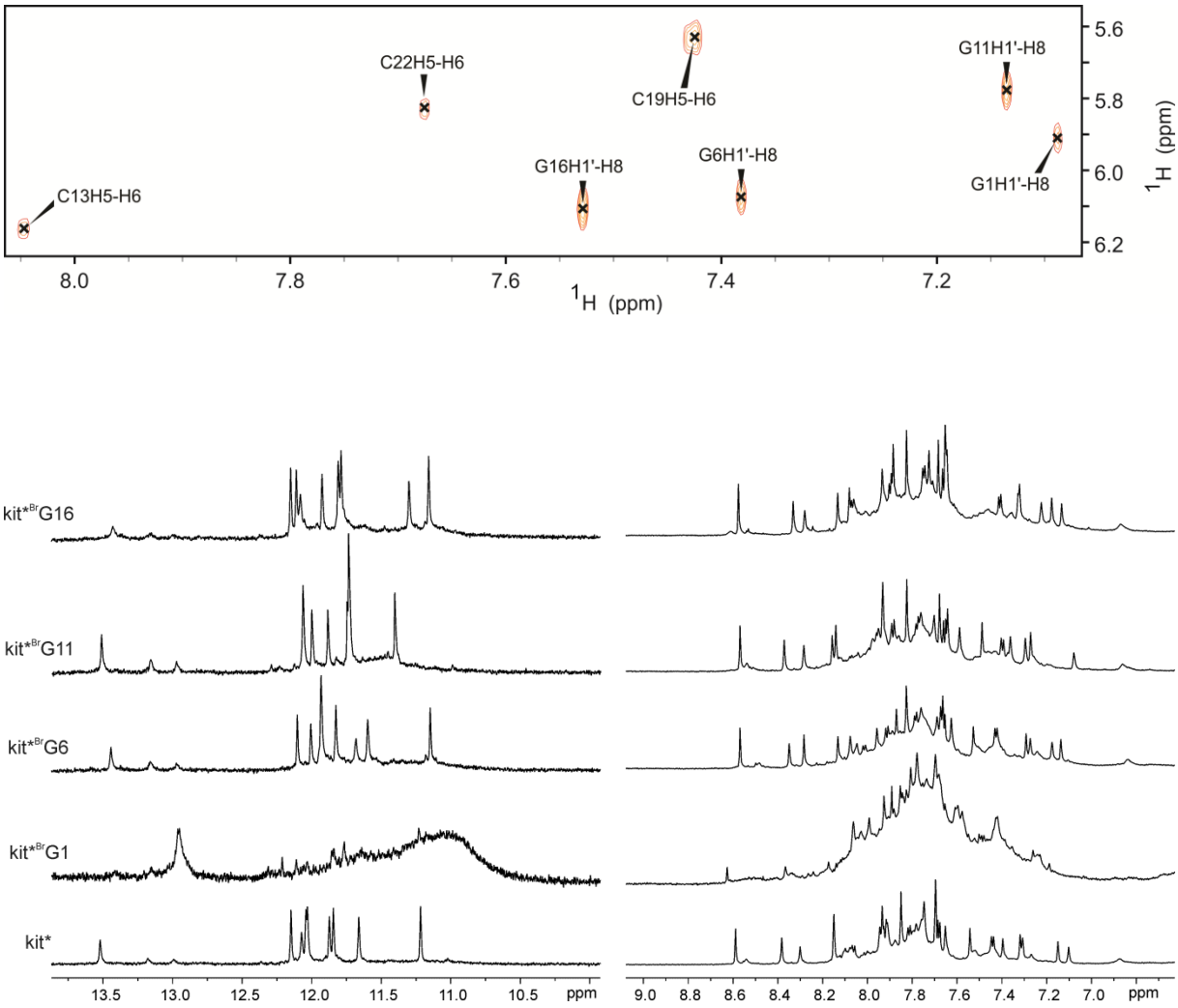

Figure S20. Top) Aromatic-anomeric region of NOESY spectrum (τ_m 40 ms) of kit*. NMR spectrum was recorded at 0.5 mM kit* kit* concentration per strand, 100 mM KCl, pH 7.4, 37°C on an 800 MHz spectrometer. **Bottom)** Imino and aromatic regions of ^{1}H NMR spectra of kit* and its analogues with single substitution of dG with 8Br-dG at positions 1, 6, 11 and 16 as indicated on the left. NMR spectra were recorded at ~0.4 mM kit* concentration per strand, 100 mM KCl, pH 7.4, at 37°C on a 600 MHz NMR spectrometer.

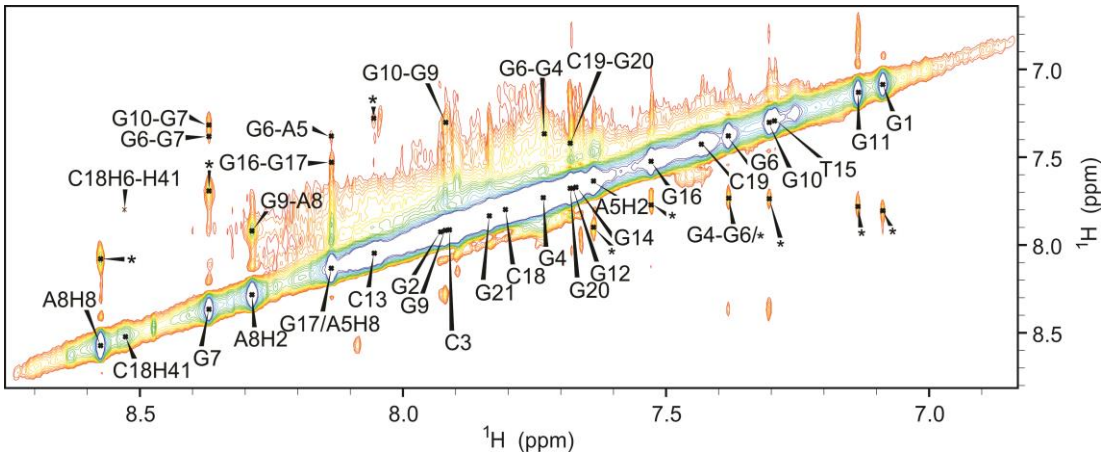

Figure S21. Aromatic-aromatic region of NOESY spectrum (τ_m 450 ms) of kit*. NMR spectrum was recorded at 0.5 mM kit* concentration per strand, 100 mM KCl, pH 7.4, 37°C on an 800 MHz spectrometer. Unambiguously assigned cross-peaks are marked above the diagonal of NOESY spectrum. Signals that could not be assigned due to overlapping or are assigned to pre-folded structure are marked with asterisks.

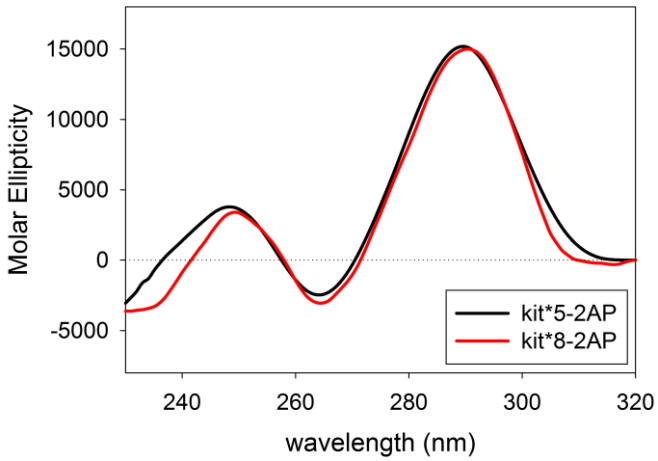

Figure S22. CD spectra of kit*5-2AP and kit*8-2AP in 10 mM TRIS, 100 mM KCl, pH 7.5 at 25 °C.

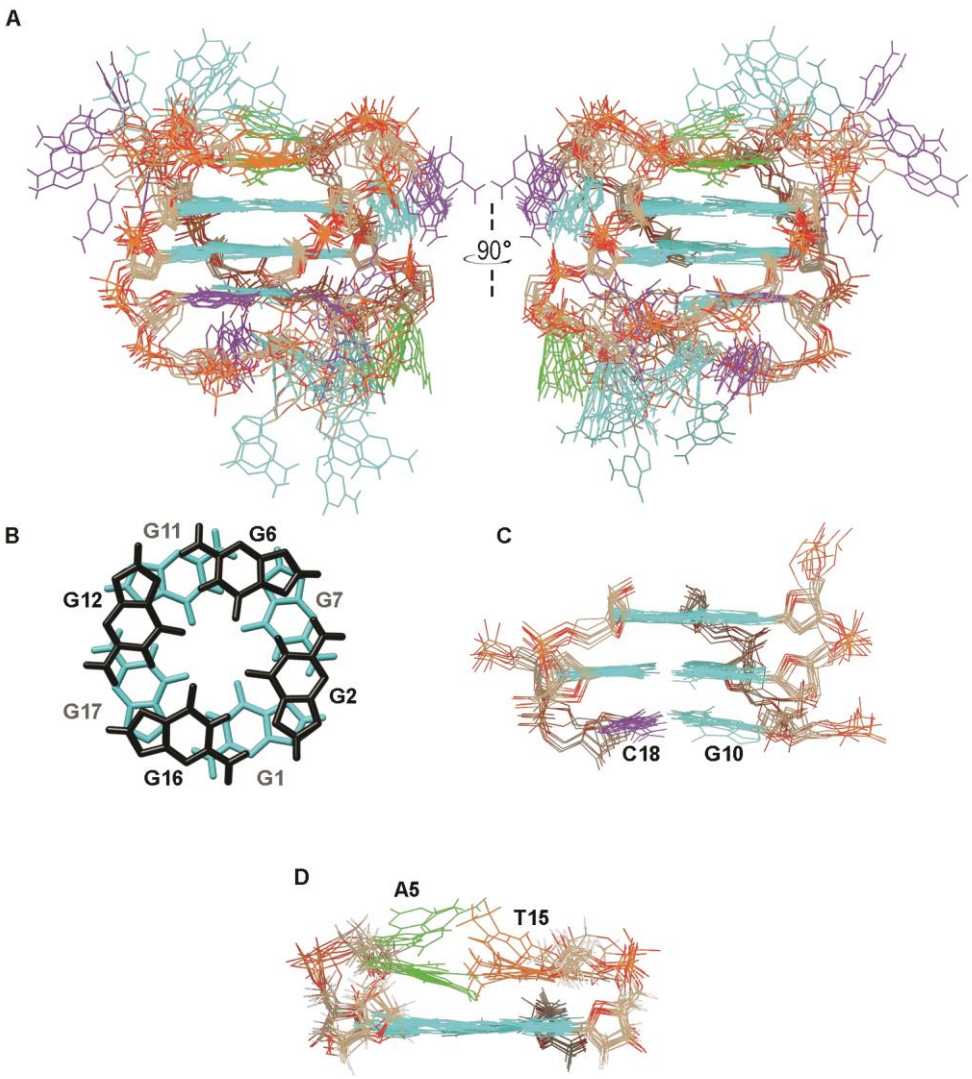

Figure S23. A) Stereoscopic view of the 10 refined superimposed structures of kit* G-quadruplex (PDB ID: 6GH0). **B**) Stacking of the two G-quartets. **C**) Side view of the G-quartet core and G10•C18 base pair stacked on the bottom G-quartet. **D**) A5 and T15 stacked on the top G-quartet.

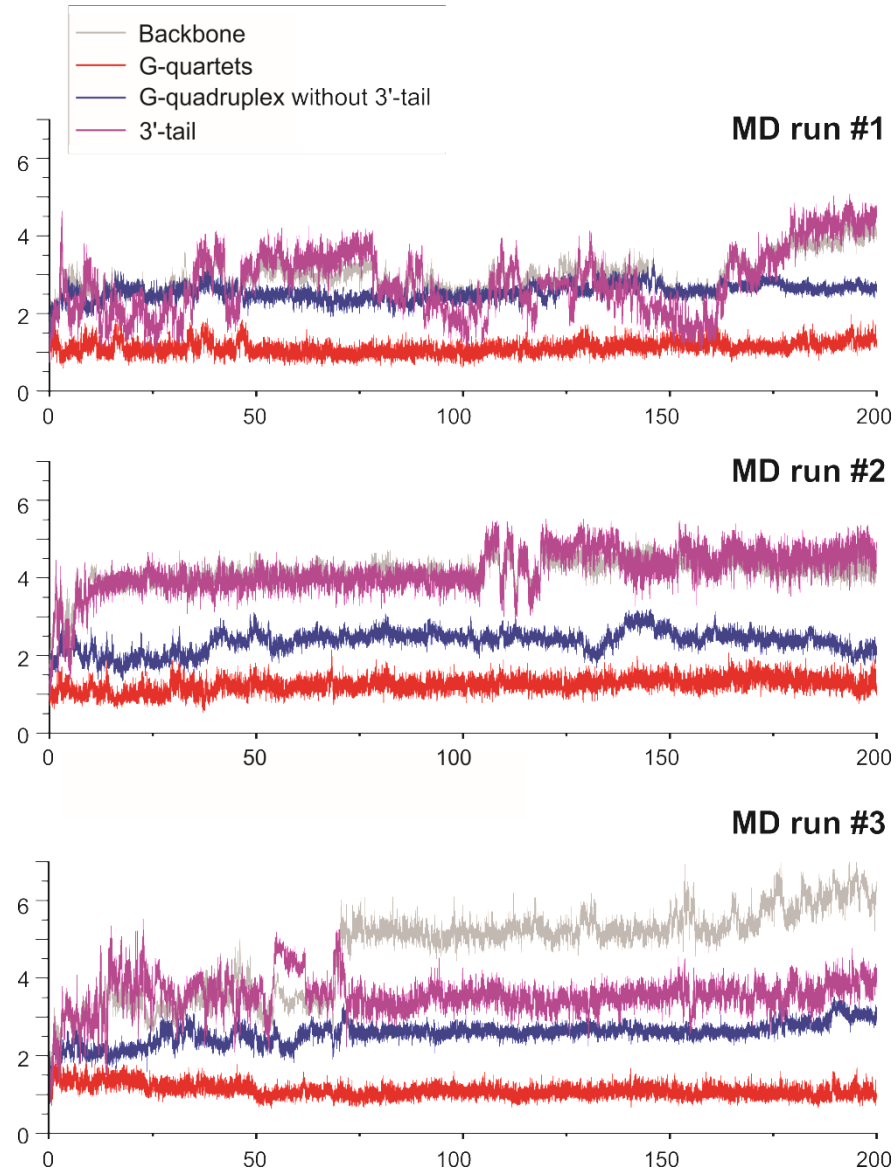

Figure S24. RMSD values of G-quadruplex backbone, G-quartet core, G-quadruplex without the 3'-tail and the 3'-tail alone as a function of simulation time during three independent 200 ns MD simulations in the presence of K^+ ions and explicit water molecules.

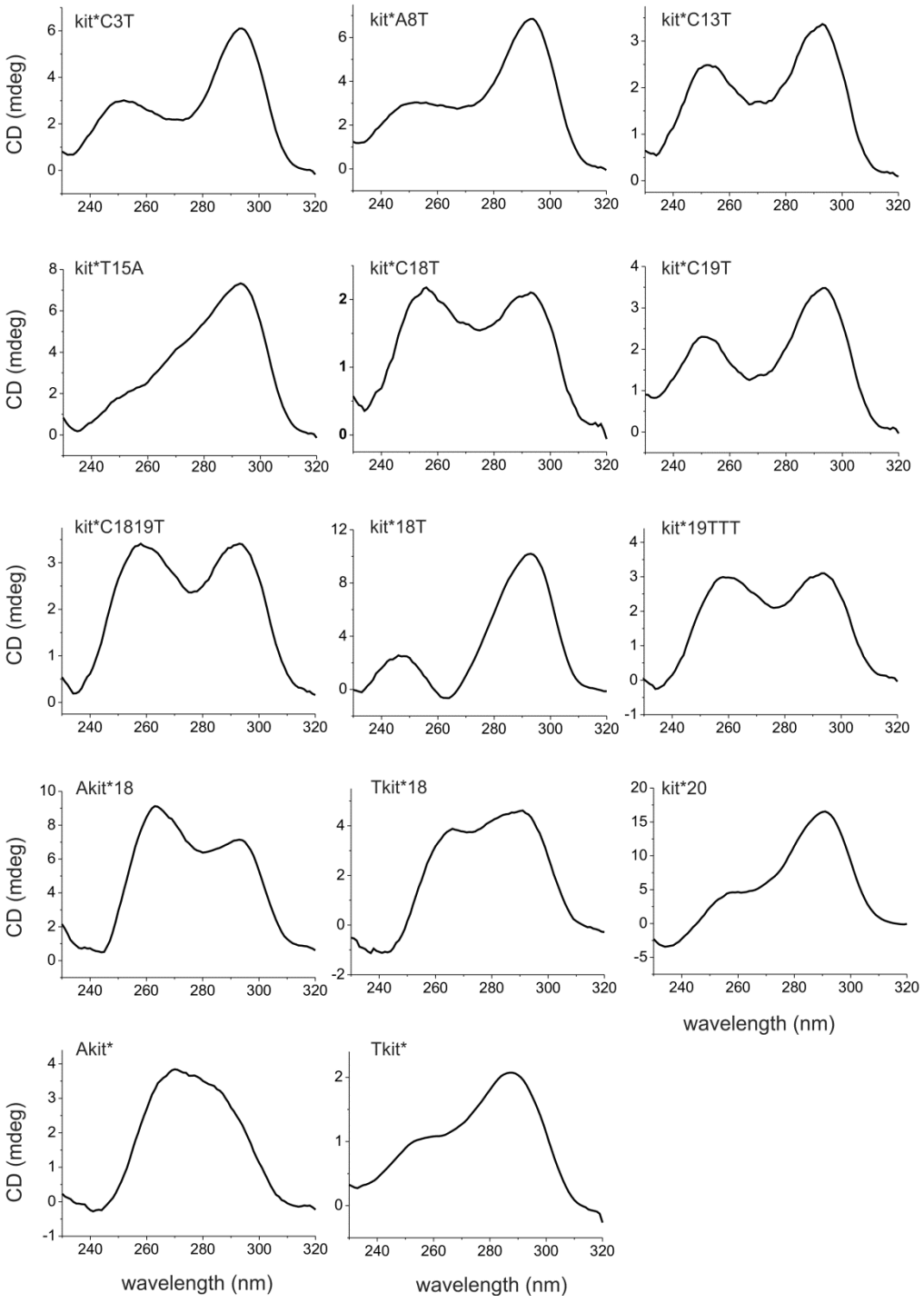

Figure S25. CD spectra of analogues of kit* oligonucleotide. CD spectra were recorded in 20 mM phosphate buffer (pH 7.4), 100 mM KCl at 37°C. The concentrations of oligonucleotides per strand were between 10 and 40 μM.

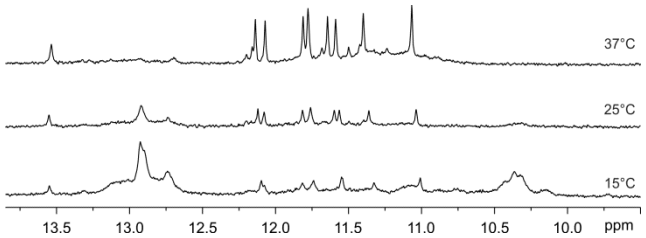

Figure S26. Imino region of ^{1}H NMR spectra of kit*T15A. NMR spectra were recorded at 20 mM phosphate buffer (pH 7.4), 100 mM KCl on a 600 MHz spectrometer.

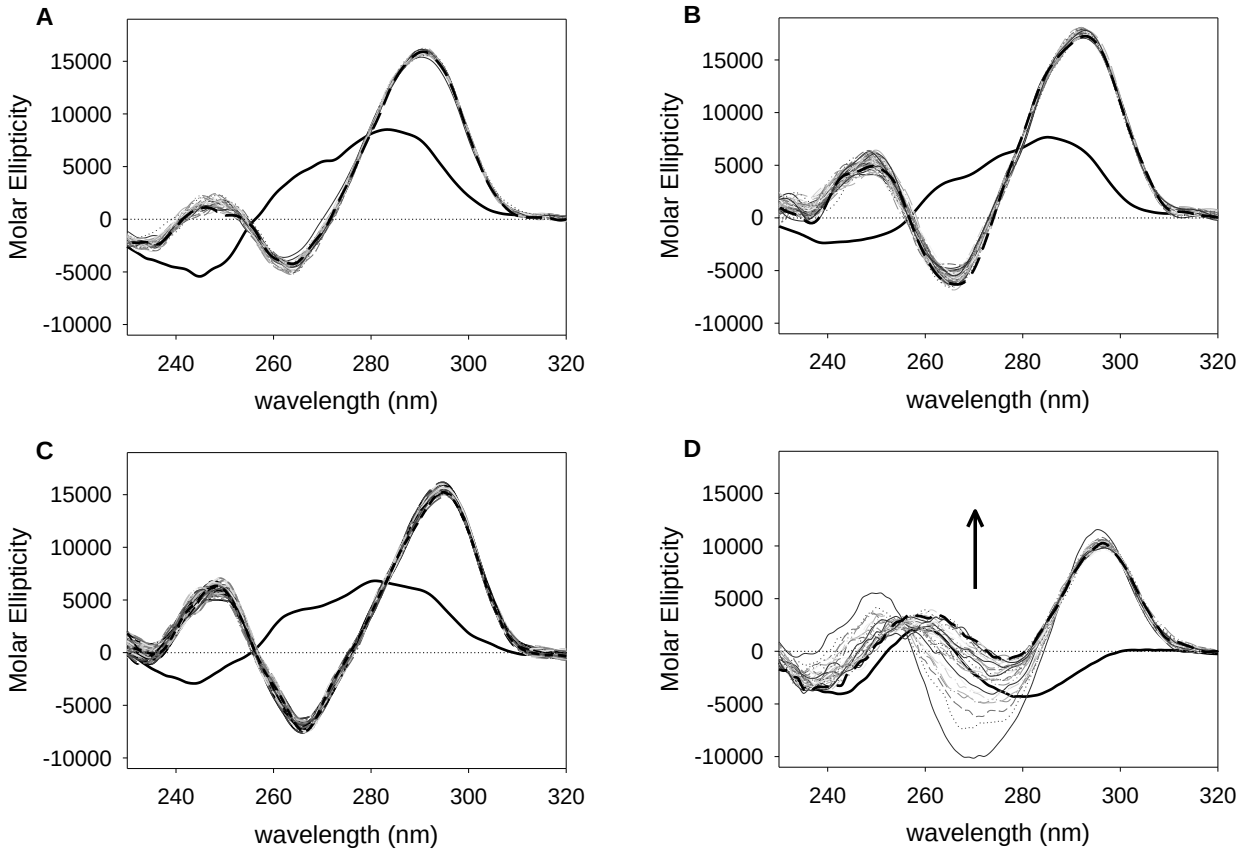

Figure S27. Time-dependent variation of CD spectra of **A**) kit*, **B**) kit*19, **C**) kit*18 and **D**) kit*17 recorded in 10 mM TRIS, pH 7.5, induced by the addition of 150 mM KCl at 37°C. The solid black lines correspond to CD spectra in the absence of K^{+} ions; the black dashed lines are related to dichroic signals after 15 hours upon addition of KCl.

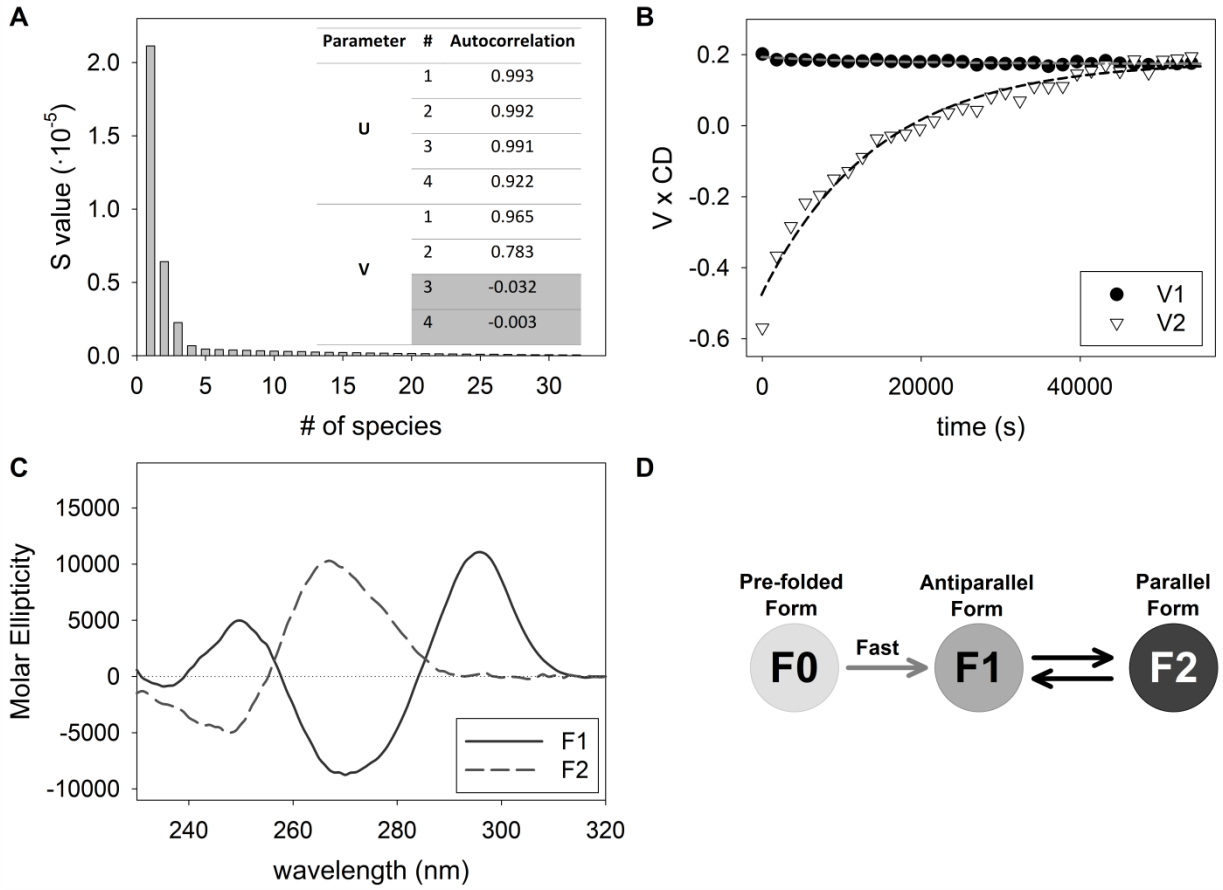

Figure S28. SVD analysis of CD folding kinetics of kit*17 promoted by 150 mM KCl. **A**) S matrix values and autocorrelation coefficients of U and V matrices indicating the relevance of species in solution participating to the overall dichroic signal variations along time. **B**) Plot of the significant V eigenvectors as a function of time and their global fitting by using mono-exponential kinetic model. **C**) CD spectra of species in solution that contribute to the overall changes of the dichroic signal as derived from SVD analysis. **D**) Proposed scheme of folding of kit*17.

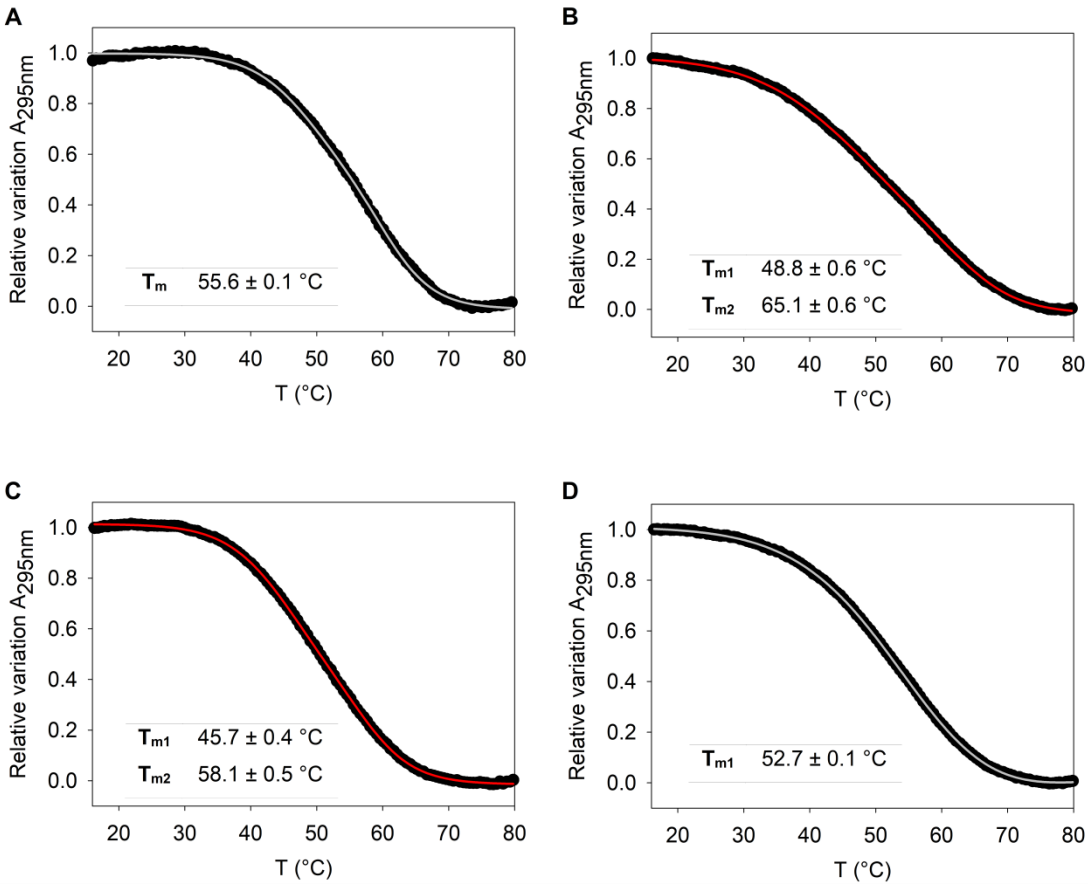

Figure S29. Thermal profiles of A) kit*, B) kit*17, C) kit*18 and D) kit*19. The UV spectra were recorded at 20 μM concentration of an oligonucleotide per strand, in 20 mM potassium phosphate buffer (pH 7.4) and 100 mM KCl. Data points were fitted by applying Equations 3 and 4 to obtain the best fit. Melting temperatures are reported in the graphs.

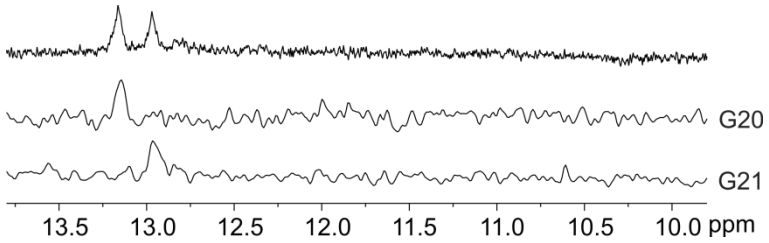

Figure S30. Imino region of ^{1}H and 1D ^{15}N-edited HSQC NMR spectra of pre-folded state of kit* (pre-kit*). The HSQC spectra were acquired on partially (10%) residue-specifically ^{15}N- and ^{13}C-labeled oligonucleotides. Assignment of H1 proton resonances is indicated on the right of each 1D HSQC spectrum. NMR spectra were recorded at 0.5 mM kit* concentration per strand, 100 mM KCl, pH 7.4, 37°C on a 600 MHz spectrometer.

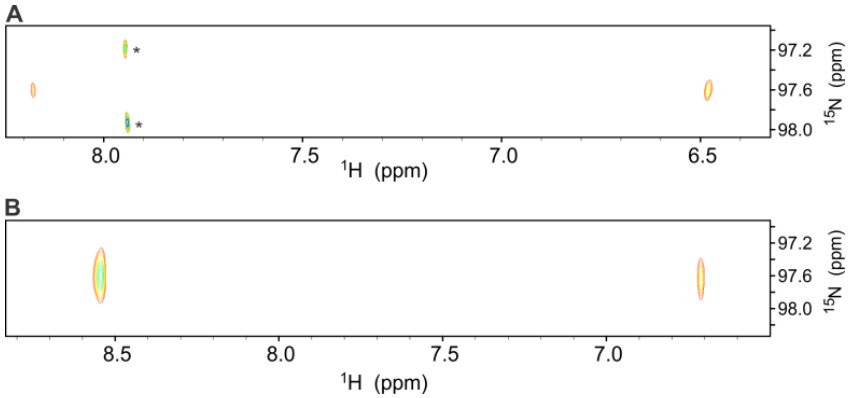

Figure S31. 2D ^{15}N-edited HSQC NMR spectrum of amino group of **A**) C18 and **B**) C19 residues of pre-kit*. The HSQC spectrum was acquired on partially (4%) residue-specifically ^{15}N- and ^{13}C-labeled oligonucleotide. NMR spectrum was recorded at 0.5 mM kit* concentration per strand, 37°C on a 600 MHz spectrometer. The signals in **A**) marked with asterisks are the F1 artifacts.

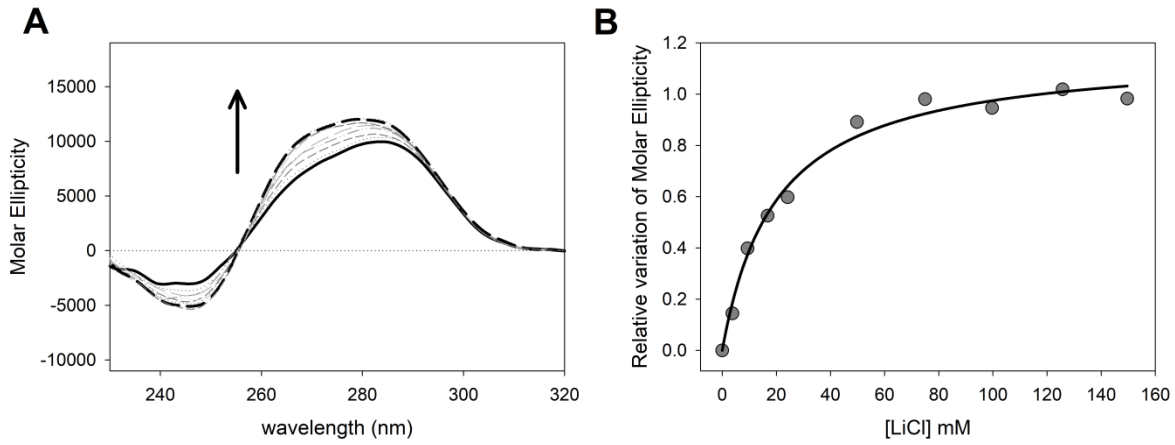

Figure S32. A) CD spectra of kit* titrated with increasing concentration of LiCl in 10 mM TRIS, pH 7.5 at 25°C. **B**) Relative variation of molar ellipticity obtained monitoring the spectral changes induced by the addition of LiCl at 266 nm. Data were fitted according to one-site saturation model (Equation 1). The obtained K_D value is 19.9 ± 2.4 mM.

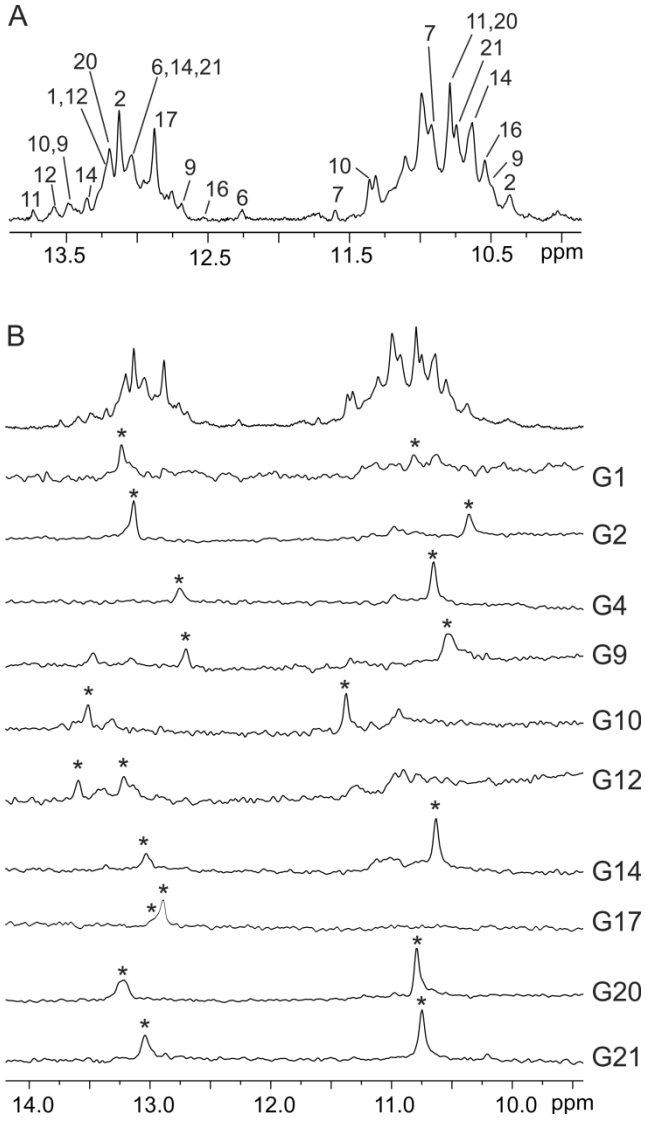

Figure S33. A) Imino region of ^{1}H NMR spectra of pre-folded states of kit*. Assignments are shown above individual signals. **B**) Imino region of ^{1}H and 1D ^{15}N-edited HSQC NMR spectra of pre-folded states of kit*. The HSQC spectra were acquired on partially (10%) residue-specifically ^{15}N- and ^{13}C-labelled oligonucleotides. Assignment of H1 proton resonances is indicated on the right of each 1D HSQC spectrum. For G6, G7, G11 and G16 residues the 2D ^{15}N-edited HSQC NMR spectra were recorded to obtain better resolution (not shown). NMR spectra were recorded at 0.5 mM kit* concentration per strand, 100 mM KCl, pH 7.4, 5°C on a 600 MHz spectrometer.

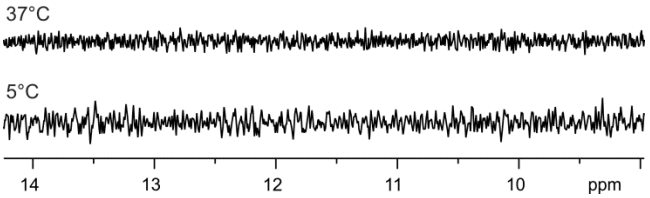

Figure S34. Imino region of ^{1}H NMR spectra of *c* construct at 37 and 5°C. NMR spectra were recorded at 0.3 mM concentration of DNA on a 600 MHz spectrometer.

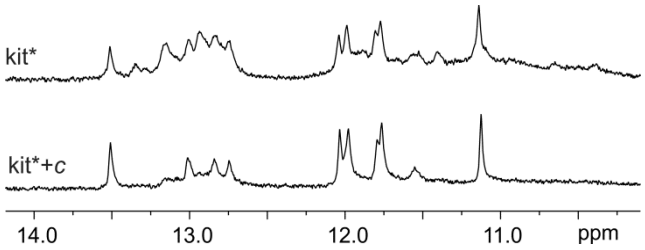

Figure S35. Imino region of ^{1}H NMR spectra of kit* and kit*+*c* at 5°C. NMR spectra were recorded at 100 mM KCl, pH 7.4 on an 800 MHz spectrometer.

Table S1. ^{1}H NMR chemical shifts of kit* G-quadruplex.[a]

Proton	H6/H8	H1/H2 H5/Me	H1'	H2'/H2"	H3'	H4'	H5'/H5"
Residue							
G1	7.09	12.13	5.91	2.85/2.90	5.01	4.36	4.15
G2	7.93	12.06	5.63	2.51	5.01	4.36	4.15
C3	7.91	5.87	6.24	2.12/2.73	n.a.	4.36	4.11
G4	7.73	/	5.74	2.22	4.86	4.29	4.13
A5	8.14	7.64	6.19	2.66	4.84	n.a.	4.17
G6	7.38	11.83	6.08	3.38/2.91	4.83	4.33	3.78/3.64
G7	8.37	11.86	6.25	2.98/2.60	5.21	4.96	4.34
A8	8.57	8.29	6.59	3.04	4.84	4.49	4.18
G9	7.92	/	5.92	1.88	4.81	4.36	4.05
G10	7.30	13.50	5.89	2.54/3.02	5.08	4.79	4.22/4.23
G11	7.14	11.20	5.78	2.67/3.05	4.96	4.37	4.20
G12	7.68	11.65	6.13	2.50/2.71	4.83	4.51	4.11
C13	8.05	6.16	6.35	2.22/2.65	4.89	4.41	4.25
G14	7.66	/	5.76	2.29	4.89	4.26	4.08
T15	7.29	1.67	5.85	2.11/2.51	4.68	4.05	3.18/3.74
G16	7.53	12.03	6.11	2.94/3.47	4.91	4.51	4.30/4.07
G17	8.14	12.02	5.78	2.73/2.53	5.04	4.51	4.30
C18	7.80	5.53	6.30	2.34/2.62	4.82	4.35	4.28
C19	7.43	5.63	5.96	1.88/2.34	4.81	4.26	4.10
G20	7.68	/	5.73	2.45	4.84	n.a.	4.05
G21	7.84	/	6.00	2.67/2.53	4.89	4.22	4.06
C22	7.68	5.82	6.11	2.32	5.01	n.a.	n.a.

[a] ^{1}H NMR chemical shifts given in ppm were measured in 90% H_2O / 10% $^{2}H_2O$, 37 °C, 0.5 mM concentration of kit* oligonucleotide per strand, 100 mM KCl and 20 mM potassium phosphate buffer (pH 7.4) and referenced to TMS. "n.a." stands for not assigned chemical shifts.

Table S2. Structural statistics for G-quadruplex structure adopted by kit*

NMR distance and torsion angle restraints	
NOE-derived distance restraints	
Total	233
Intra-residue	172
Inter-residue	61
Sequential	53
Long-range	8
Hydrogen bond restraints	18
Torsion angle restraints	22
G-quartet planarity restraints	24
Structure statistics	
Violations	
Mean NOE restraint violation (Å)	0.10 ± 0.03
Max NOE restraint violation (Å)	0.18
Max torsion angle NOE restraint violation (°)	3.04
Deviation from idealized geometry	
Bonds (Å)	0.01 ± 0.00
Angles (°)	2.50 ± 0.04
Pairwise heavy atom RMSD (Å)	
Overall	2.63 ± 0.32
G-quartets	0.80 ± 0.17
G-quartets and G10•C18	0.88 ± 0.17
G-quartets, A5 and T15	1.32 ± 0.32

REFERENCES

1. DeSa, R.J. and Matheson, I.B. (2004) A practical approach to interpretation of singular value decomposition results. *Methods Enzymol.*, **384**, 1-8.
2. Hendler, R.W. and Shrager, R.I. (1994) Deconvolutions based on singular value decomposition and the pseudoinverse: a guide for beginners. *J. Biochem. Biophys. Methods*, **28**, 1-33.
3. Gray, R.D., Buscaglia, R. and Chaires, J.B. (2012) Populated intermediates in the thermal unfolding of the human telomeric quadruplex. *J. Am. Chem. Soc.*, **134**, 16834-16844.
4. Greenfield, N.J. (2006) Using circular dichroism collected as a function of temperature to determine the thermodynamics of protein unfolding and binding interactions. *Nat. Protoc.*, **1**, 2527-2535.
5. Gray, R.D., Petraccone, L., Buscaglia, R. and Chaires, J.B. (2010) 2-aminopurine as a probe for quadruplex loop structures. *Methods Mol. Biol.*, **608**, 121-136.
6. Wang, J., Wolf, R.M., Caldwell, J.W., Kollman, P.A. and Case, D.A. (2004) Development and testing of a general amber force field. *J. Comput. Chem.*, **25**, 1157-1174.
7. Salomon-Ferrer, R., Götz, A.W., Poole, D., Le Grand, S. and Walker, R.C. (2013) Routine Microsecond Molecular Dynamics Simulations with AMBER on GPUs. 2. Explicit Solvent Particle Mesh Ewald. *J. Chem. Theory Comput.*, **9**, 3878-3888.
8. Case, D.A., Berryman, J.T., Betz, R.M., Cerutti, D.S., T.E. Cheatham, T.E., III,, Darden, T.A., Duke, R.E., Giese, T.J., Gohlke, H., Goetz, A.W. *et al.* (2015) AMBER 2015, University of California, San Francisco.
9. Cornell, W.D., Cieplak, P., Bayly, C.I., Gould, I.R., Merz, K.M., Ferguson, D.M., Spellmeyer, D.C., Fox, T., Caldwell, J.W. and Kollman, P.A. (1996) A second generation force field for the simulation of proteins, nucleic acids, and organic molecules. *J. Am. Chem. Soc.*, **118**, 2309-2309.
10. Perez, A., Marchan, I., Svozil, D., Sponer, J., Cheatham, T.E., 3rd, Laughton, C.A. and Orozco, M. (2007) Refinement of the AMBER force field for nucleic acids: improving the description of alpha/gamma conformers. *Biophys. J.*, **92**, 3817-3829.

11. Krepl, M., Zgarbova, M., Stadlbauer, P., Otyepka, M., Banas, P., Koca, J., Cheatham, T.E., 3rd, Jurecka, P. and Sponer, J. (2012) Reference simulations of noncanonical nucleic acids with different chi variants of the AMBER force field: quadruplex DNA, quadruplex RNA and Z-DNA. *J. Chem. Theory Comput.*, **8**, 2506-2520.
12. Zgarbova, M., Luque, F.J., Sponer, J., Cheatham, T.E., 3rd, Otyepka, M. and Jurecka, P. (2013) Toward Improved Description of DNA Backbone: Revisiting Epsilon and Zeta Torsion Force Field Parameters. *J. Chem. Theory Comput.*, **9**, 2339-2354.
13. Zgarbova, M., Sponer, J., Otyepka, M., Cheatham, T.E., 3rd, Galindo-Murillo, R. and Jurecka, P. (2015) Refinement of the Sugar-Phosphate Backbone Torsion Beta for AMBER Force Fields Improves the Description of Z- and B-DNA. *J. Chem. Theory Comput.*, **11**, 5723-5736.
14. Onufriev, A., Bashford, D. and Case, D.A. (2000) Modification of the generalized Born model suitable for macromolecules. *J. Phys. Chem. B*, **104**, 3712-3720.
15. Onufriev, A., Bashford, D. and Case, D.A. (2004) Exploring protein native states and large-scale conformational changes with a modified generalized born model. *Proteins*, **55**, 383-394.
16. Ryckaert, J.P., Ciccotti, G. and Berendsen, H.J.C. (1977) Numerical integration of Cartesian equations of motion of a system with constraints: molecular dynamics of *n*-alkanes. *J. Comput. Phys.*, **23**, 327-341.
17. Neidle, S. (2010) *Principles of Nucleic Acid Structure*. Academic Press:, London.
18. Pettersen, E.F., Goddard, T.D., Huang, C.C., Couch, G.S., Greenblatt, D.M., Meng, E.C. and Ferrin, T.E. (2004) UCSF Chimera--a visualization system for exploratory research and analysis. *J. Comput. Chem.*, **25**, 1605-1612.
19. Ding, Y., Fleming, A.M., He, L. and Burrows, C.J. (2015) Unfolding Kinetics of the Human Telomere i-Motif Under a 10 pN Force Imposed by the α-Hemolysin Nanopore Identify Transient Folded-State Lifetimes at Physiological pH. *J. Am. Chem. Soc.*, **137**, 9053-9060.
20. Phan, A.T., Kuryavyi, V., Gaw, H.Y. and Patel, D.J. (2005) Small-molecule interaction with a five-guanine-tract G-quadruplex structure from the human MYC promoter. *Nat. Chem. Biol.*, **1**, 167-173.
21. Stefl, R., Oberstrass, F.C., Hood, J.L., Jourdan, M., Zimmermann, M., Skrisovska, L., Maris, C., Peng, L., Hofr, C., Emeson, R.B. *et al.* (2010) The Solution Structure of the ADAR2 dsRBM-RNA Complex Reveals a Sequence-Specific Readout of the Minor Groove. *Cell*, **143**, 225-237.
22. Kotar, A., Wang, B., Shivalingam, A., Gonzalez-Garcia, J., Vilar, R. and Plavec, J. (2016) NMR Structure of a Triangulenium-Based Long-Lived Fluorescence Probe Bound to a G-Quadruplex. *Angew. Chem. Int. Ed. Engl.*, **55**, 12508-12511.
23. Darden, T., York, D. and Pedersen, L. (1993) Particle Mesh Ewald - an N.Log(N) Method for Ewald Sums in Large Systems. *J. Chem. Phys.*, **98**, 10089-10092.
24. Essmann, U., Perera, L., Berkowitz, M.L., Darden, T., Lee, H. and Pedersen, L.G. (1995) A smooth particle mesh Ewald method. *J. Chem. Phys.*, **103**, 8577-8593.